Saudi Dental Journal (2022) **34**, 485–493

King Saud University

Saudi Dental Journal

www.ksu.edu.sa
www.sciencedirect.com

ORIGINAL ARTICLE

Osteogenic potential of calcium silicate-doped iron oxide nanoparticles versus calcium silicate for reconstruction of critical-sized mandibular defects: An experimental study in dog model

Said K. Taha [a], Mohamed A. Abdel Hamid [b], Esmat M.A. Hamzawy [c], Sayed H. Kenawy [d], Gehan T. El-Bassyouni [d], Elham A. Hassan [b,*], Heba E. Tarek [e]

[a] *Surgery and Oral Medicine Department, Oral and Dental Research Institute, National Research Centre, 33 El Buhouth St, Dokki, Giza 12622, Egypt*
[b] *Department of Surgery, Anesthesiology and Radiology, Faculty of Veterinary Medicine, Cairo University, Giza 12211, Egypt*
[c] *Glass Research Department, Advanced Materials Technology and Mineral Resources Research Institute, National Research Centre, 33 El Buhouth St, Dokki, Giza, 12622, Egypt*
[d] *Refractories, Ceramics and Building Materials Department, Advanced Materials Technology and Mineral Resources Research Institute, National Research Centre, 33 El Buhouth St., Dokki, Giza 12622, Egypt*
[e] *Basic Dental Science Department, Oral and Dental Research Institute, National Research Centre, 33 El Buhouth St, Dokki, Giza 12622, Egypt*

Received 27 September 2021; revised 22 June 2022; accepted 23 June 2022
Available online 28 June 2022

KEYWORDS

Calcium silicate;
Iron oxide nanoparticles;
Mandible;
Defect;
Bone regeneration;
Dog

Abstract *Objective:* To evaluate bioactivity and osteogenic potential of calcium silicate (CS)-doped iron oxide (Fe_2O_3) nanoparticles versus pure CS in the reconstruction of induced critical-sized mandibular defects.

Design: CS-doped Fe_2O_3 was prepared; morphological and microstructure identification of nanoparticles were made. An *in vivo* randomised design was developed on 24 adult male dogs where four critical-sized mandibular defects were created in each dog. Bone defects were allocated into control, CS, CS-3% Fe_2O_3 and CS-10% Fe_2O_3 group. Dogs were euthanized at 1 and 3 months (12 dog/time) for histopathologic and histomorphometric evaluation.

Results: At three months, bone formation and maturation were evident where mean ± SD percent of mature bone was 2.66 ± 1.8, 9.9 ± 2.5, 22.9 ± 4.9, and 38.6 ± 8.1 in control, CS, CS-3%

* Corresponding author.
E-mail address: elhamhassan@cu.edu.eg (E.A. Hassan).
Peer review under responsibility of King Saud University.

Production and hosting by Elsevier

https://doi.org/10.1016/j.sdentj.2022.06.008

Fe_2O_3, and CS-10% Fe_2O_3 groups respectively. A high significant ($P < 0.001$) increase in area percent of mature bone was recorded in CS, CS-3% Fe_2O_3, and CS- 10% Fe_2O_3 groups compared to control group (73%, 88% and 93.3% respectively). Significant increase ($P < 0.001$) in area of mature bone was recorded in CS-3% Fe_2O_3 and CS-10% Fe_2O_3 groups compared to CS group. A significant increase ($P < 0.001$) in area of mature bone formation was detected in CS-10% Fe_2O_3 group compared to other groups.

Conclusion: CS-doped Fe_2O_3 has good osteoconductive, biocompatible properties with promoted bone regeneration. Fe_2O_3 has synergistic effect in combination with CS to promote bone formation. Increasing concentration of Fe_2O_3 nanoparticles resulted in improved osteogenesis and maturation. Results suggests that the novel CS-Fe_2O_3 alloplasts could be used for reconstruction of critical-sized bone defects.

1. Introduction

Bone defects represent a major challenge for maxillofacial surgeons (Altwaim et al., 2021). Critical-sized bone defects are those intraosseous gaps exceeding the body's ability of self-regeneration (Schmitz and Hollinger, 1986). Bone formation is limited to tiny bony clusters on the defect's margin while the defect itself will be occupied by fibrous tissue of inferior structural and functional properties (Altwaim et al., 2021). Critical-sized bone defects necessitate an assisted regeneration to obtain optimum regeneration (Taha et al., 2010, 2018). Bone grafting had been widely used, however donor site morbidity, graft harvesting procedures and the need of extra-surgery are limiting factors (Alasmari and Dhaifullah, 2019). Bone tissue engineering can provide synthetic substitutes to restore damaged bone. It provides three-dimensional natural and/or synthetic scaffolds with excellent biocompatible, bioresorbable, osteoconductive and osteoinductive properties (Wu et al., 2006).

Calcium silicate (CS) is an alloplast used for guided bone regeneration. It provides matrix for bone ingrowth while it resorbs in appropriate time required for regeneration. CS had significant effect on osteoblastic differentiation and osteoclastic resorption (Wei et al., 2009). The rate of apatite formation induced by CS-biomaterials exceeds that induced by biocompatible bioglass. Although CS have significant bioactivity, they are very brittle and difficult in processing (Wu et al., 2006).

Metals and metal ions were used as dopant material for bone regeneration providing structural and functional support. Nano-porous materials with high specific surface area acquired great interests in biomedical applications. Increase of surface area and pore volume might greatly increase kinetic process of apatite formation and consequently improve bone-forming bioactivity (Hong et al., 2009, 2010).

Wollastonite ($CaSiO_3$) is Ca-Si based bioceramic that has been investigated as bioactive material for bone regeneration. It has excellent bioactivity and degradability beside being osteoconductive and noncytotoxic (Mabrouk et al., 2019, 2021).

There are limited studies reporting the nanostructure created by doping Fe_2O_3 with calcium silicate and its role in bone regeneration. The present study aimed to evaluate bioactivity and osteogenic potential of calcium silicate doped with Fe_2O_3 nanoparticles for reconstruction of experimentally induced mandibular defects in dogs.

2. Materials and methods

2.1. Preparation of calcium silicate-doped iron oxide

Stoichiometric wollastonite ($CaSiO_3$) was prepared with incorporation of Fe_2O_3 through wet method. Calcium carbonate ($CaCO_3$, 99%, El-Gomhorya Co., Egypt), silica gel (SiO_2, Fluka) and iron nitrate [$Fe(NO_3)_3$, 99.9%] were engaged as sources of Ca^{2+}, SiO_2 and Fe^{3+} respectively. Analytical nitric acid (HNO_3) and ammonia solution (25%) were used. Two individual weight % concentrations of Fe^{3+} (3 and 10) above/100 g of $CaSiO_3$ slurry were produced (Mabrouk et al., 2021). Slurry was left to age while magnetic stirring to ensure comprehensive mixing; then dried and the resulting powder was ball milled and sieved into fine powder <0.037 mm. Powder was shaped through uniaxial pressure (20KN) using PVA (7%) solution as a binder into green discs. The discs were sintered in Vectstar furnaces at 1000 ℃ for 2 hr. Wollastonite was prepared using the following equations (Mabrouk et al., 2019).

$$- CaCO_3 + 2\,HNO_3 \xrightarrow{Heat} Ca(NO_3)_2 + H_2O + CO_2\uparrow$$

$$- Ca(NO_3)_{2\ solu.} + SiO_2{\cdot}nH_2O_{powder} \xrightarrow{drying-Calcination\ at\ 550^{\circ}C/2h-1000^{\circ}C/2h} CaSiO_3\ powder$$

$$- Ca(NO_3)_{2\ solu.} + SiO_2{\cdot}nH_2O_{powder} + H_2O + Fe(NO_3)_3\ solution \xrightarrow{Stirring\ for\ 2\ h-drying}$$

$$- Ca(NO_3)_{2\ solu.} + SiO_2{\cdot}nH_2O_{powder} + Fe(NO_3)_3 \xrightarrow{Calcination\ at\ 550^{\circ}C/2h-1000^{\circ}C/2h} CaSiO_3/(Fe_2O_3)$$

Identification of crystalline phases after sintering was made using X-ray diffraction analysis (XRD) in the range of $2\theta = 5–60°$ (Empyrean Panalytical diffractometer system, USA). Morphology and microstructure of samples were detected via field emission scanning electron microscopy (FE-SEM, Philips model-FEG Quanta 250, Holland). The sintered sample was etched in dilute solution of 1 %HNO_3 + 1 %HF for 30 s before scanning. Wet chemical etching is a common strategy for glass microfabrication. It refers to removal or dissolving of material from a substrate when immersed in liquid etchant. HF is used as a main etchant for silicate glass and HNO3 was added to con-

trol etching rate. Fourier transformer infrared spectrophotometer (FT-IR) (Model FT/IR- 6100 type A, Germany) was used to elucidate the effect of Fe_2O_3 on physicochemical properties of Fe_2O_3-doped nanoparticles. Spectra were verified at wavenumbers range of 400–4000 cm-^{1}. 1 mg of sample was cautiously mixed with 200 mg of KBr and palletized under vacuum before FTIR testing. A fine powder of size < 0.037 mm was pressed into green discs through uniaxial pressure (20KN) using polyvinyl alcohol (7% PVA) solution as binder. Discs were sintered at 1000℃ for 2 hr to be used in the *in vivo* model.

2.2. In vivo study

2.2.1. Animals

Twenty-four mature male mongrel dogs (19.1 ± 2.4 month, 20.3 ± 2.1 kg) were used. Clinical and hematological examinations were done to exclude systemic and bone disease. Dogs were kept in separate cages, given free access to water, and fed twice daily. The study was approved by Animal Care and Use Ethical Committee of the National Research Center (approval #18121).

2.2.2. Study design:

A randomised controlled experimental design was planned. Under general anaesthesia, four cylindrical critical-sized (15 mm diameter, 4 mm depth) mandibular defects were induced in both mandibles of all dogs. These defects were randomly assigned to one of the following groups:

Control group (Control group): the defect was kept empty without grafting, Calcium silicate group (CS group): defect was reconstructed using pure calcium silicate, Calcium silicate-3% Fe_2O_3 group (CS- 3% Fe_2O_3 group): defect was reconstructed using calcium silicate-doped 3% Fe_2O_3, and Calcium silicate-10% Fe_2O_3 group (CS- 10% Fe_2O_3 group): defect was reconstructed using calcium silicate-doped 10% Fe_2O_3. Dogs were monitored daily and euthanized at 1 and 3 months (12 dogs/time).

2.2.3. Anesthetic protocol

Dogs were premedicated using atropine sulphate 0.1% (Atropine Sulphate®, El Nasr Pharm. Chem. Co., Egypt) 15 min before anesthesia (0.05 mg/kg s.c) and tranquilized with xylazine HCL 2% (Xylaject®, ADWIA Co., Egypt) (1 mg/kg i.m.). Anesthesia was induced by Ketamine HCL 5% (Ketalar®, Pfizer Co., Egypt) (10 mg/kg i.v.) and maintained by thiopental sodium 2.5% (Anapental®: Sigma-Tec, Egypt) (25 mg/kg i.v.).

2.2.4. Induction of critical-sized mandibular defect

A 6-cm skin incision was made below the inferior border of the mandible; dissection was continued to expose mandibular body. The periosteum was incised and elevated, a trephine bur (Trephine drill, Freiatec AG, Germany) was used to create a 15-mm circular defect. As per animal grouping, the prepared calcium silicate discs were fitted into defects (Fig. 1). Surgical wound was routinely closed including both subcutaneous tissue and skin.

2.2.5. Clinical evaluation and post-operative care

Surgical wound was dressed using 2 % povidone iodine (Betadine® Nile Pharm. Chem. Ind. Co., Egypt) for 10 days. Systemic course of antibiotic Ceftriaxone (Ceftriaxone® 1000 mg i.m., Novartis Co., Sandoz, Switzerland)1gm/dog for 7 days. Sutures were removed 12 days post-surgery. General health condition, appetite, weight loss, oral functions were evaluated.

2.2.6. Euthanasia

Dogs were humanely euthanized using an overdose of sodium pentobarbitone 200 mg (Eutha-naze®, the premier pharmaceutical Co., Sloane, Bryanston) at dose of 2 ml/kg i.v.

2.3. Histopathologic and histomorphometric evaluation

Following euthanasia, both mandibles were dissected, disarticulated, and sectioned into halves. Bone defects as well as surrounding tissue were sectioned, labelled, and sent for blind examination. Samples were sectioned at 4 μm, stained with H&E and Masson trichrome. Histomorphometric analysis as indicated by bone area percentages and area percentages of bone maturation was calculated.

2.4. Statistical analysis

Histomorphometric data were tabulated and presented as mean ± standard deviation. Normality of distribution was tested using Kolmogorov Smirnov test. A one-way analysis of variance (ANOVA) was used to compare groups. When significant differences were recorded, Post Hoc test was used for pairwise comparisons. Statistical significance was accepted when P values < 0.05. Data were analyzed using Statistical Package for Social Science (SPSS) (SPSS Inc, IBM, Chicago, IL).

3. Results:

3.1. Physicochemical evaluation

3.1.1. X-ray diffraction analysis

Wollastonite ($CaSiO_3$, ICDD-01-084-0655) was the main crystalline phase developed after sintering at 1000 °C. Traces of hematite (ICDD-73-0603 α-Fe_2O_3) were present in the 10% Fe_2O_3. The XRD pattern of samples is demonstrated in (Fig. 2a). Un-doped wollastonite demonstrated that their particles size was in the range of 10–50 nm which verified to be much greater compared with CS-3 and 10% Fe_2O_3 (10–15 nm). The presence of hematite had infected particle size, which was diminished, the existence of hematite has elevated the repulsive energy between particles and reduced their final diameters.

3.1.2. Scanning electron microscopic examination

SEM micrographs of base, 3% Fe_2O_3 and 10% Fe_2O_3 samples on the fresh fracture surface at high magnification are shown in (Fig. 2). The microstructure presented nanoparticles accumulated in irregular clusters in iron-free wollastonite (pure CS) (Fig. 2c). Sample of higher Fe_2O_3 content, grains were elucidated as irregular clusters in micro-scale encompassing some scattered light-rounded to sub-rounded nanoparticles in nano-scale size (Fig. 2d and e). SEM images revealed inhomogeneity existing on the surface of samples.

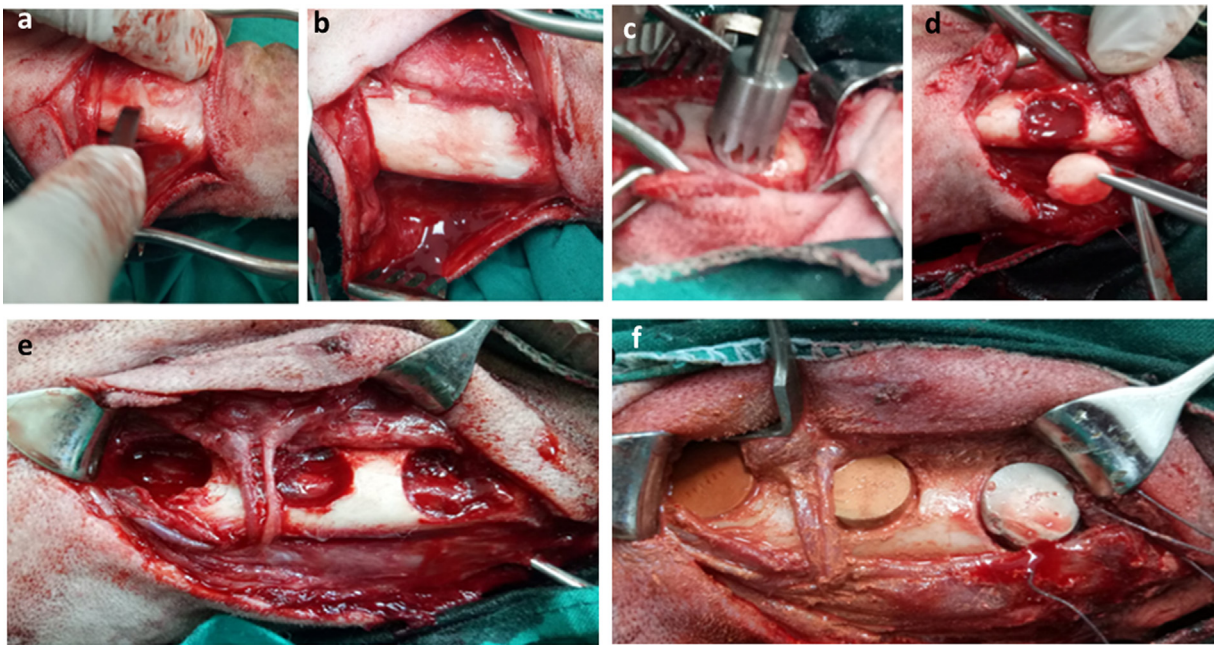

Fig. 1 Intra-operative photograph demonstrating the extra-oral approach for induction of critical-size mandibular bone defect. Skin incision was made below the inferior border of the mandible and the periosteum was incised and elevated using a periosteal elevator (a) till complete exposure of the body of the mandible (b). A trephine bur (c) was used for the induction of 15 mm circular bone defect (d). The induced defects (e) were press-fitted with cylindrical scaffold of calcium silicate or 3 % calcium silicate-doped iron oxide or 10 calcium silicate-doped iron oxide scaffold (f).

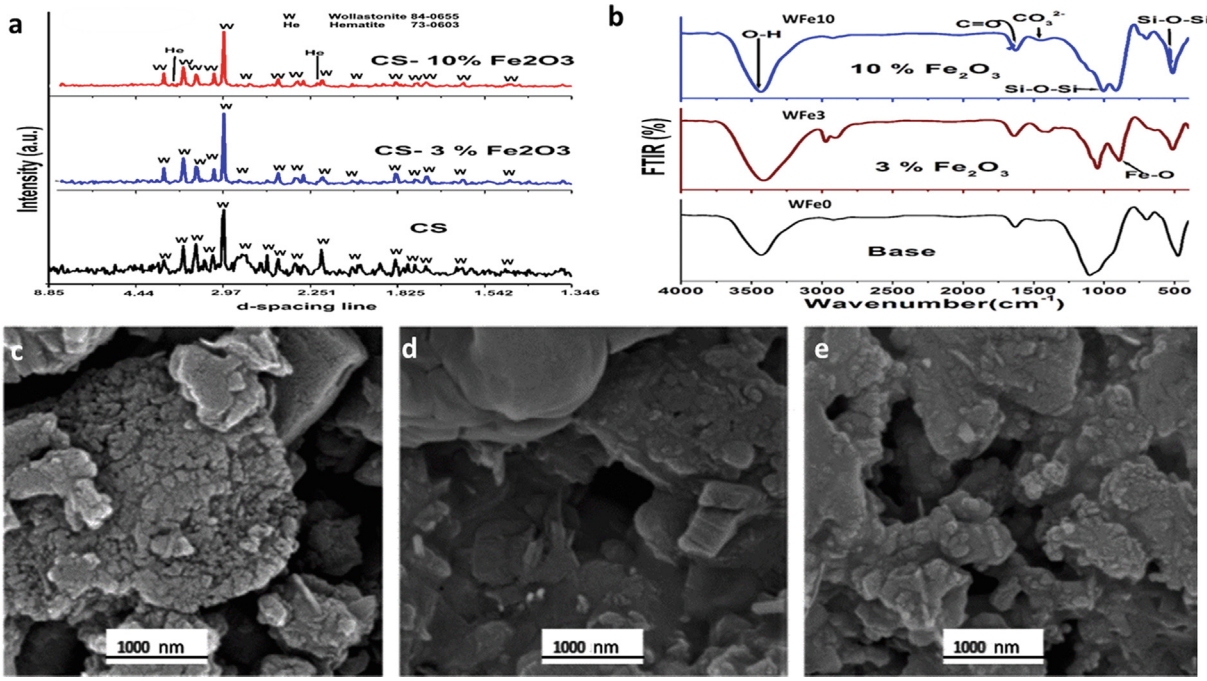

Fig. 2 X ray diffraction patterns of CS, Cs-3% Fe_2O_3, and CS-10% Fe_2O_3 samples sintered at 1000℃/2 hrs (a), FTIR spectroscopy of base CS, 3 and 10% Fe_2O_3 (b). Scanning electron microscopic micrographs of base CS (c), 3% Fe_2O_3 (d) and 10% Fe_2O_3 (e).

3.1.3. Fourier transformer infrared spectrophotometer analysis

The 4000–400 cm^{-1} spectra of sintered samples at 1000 °C/2hr are demonstrated in (Fig. 2b). For base, there was an intense broad band at 1100 cm^{-1} and few bands at 490 and 950 cm^{-1} accredited to the Si—O—Si anti-symmetric stretching of bridging oxygen within the tetrahedral. In Fe_2O_3 containing

samples there was a band at 870 cm^{-1} and a shoulder at 580 cm^{-1} attributed to Fe—O stretching vibration.

3.2. Clinical examination

No adverse or allergic reactions were recorded in any dog after surgery. Appetite, body weight, general health, and oral function were maintained.

3.3. Histopathological examination

3.3.1. H&E staining

Histopathological examination of control defects at one month revealed loose connective tissue occupying defect site while CS group had more condensed connective tissue filling the defect gap. Both CS-3% Fe_2O_3 and CS-10% Fe_2O_3 groups demonstrated new bone formation that appeared as interconnected trabeculae with loosely arranged connective tissue in between (Fig. 3 a-d).

At 3 months, bone marrow spaces, osteoblastic proliferation, and Haversian system were seen in CS-3% Fe_2O_3 and CS-10% Fe_2O_3 groups indicating regular bone formation (Fig. 3 e-h)

3.3.2. Masson trichrome staining

At one month, control defects were invaded by thin, loosely organized connective tissues with presence of only small bony spicules. In CS, CS-3% Fe_2O_3 and CS-10% Fe_2O_3 groups thin islets of bone were seen between collagen fibers. Bone regeneration occurred in a centripetal fashion from the periphery of the defect. Bone regeneration was more obvious in CS- 10% Fe_2O_3 group where the defect tended to coalesce with new bone. Evidence of newly formed bone was observed to be mixed with degraded discs that were seen as white areas between newly formed bony areas. The newly formed lamellar bone demonstrated osteons with Haversian canals. The canals contained blood vessels and erythrocytes that were stained bright red. New bone formation was elucidated at the periphery of the defect zone and white spots were seen representing the original material exposed to dissolution during bone decalcification. Osteocytes and osteoblasts were present within the newly formed bone as lining cells along the margin of the trabeculae (Fig. 4).

In all defects, necrosis, infection, fibrinous exudates, and tissue degeneration were not observed at any time. Based on the absence of adverse tissue effects and the mild tissue reaction to the used materials, healing of the defects appeared to be progressing in normal fashion.

At 3 months, the newly formed bone in CS-10% Fe_2O_3 group became nearly mature and acquired purple color as it was more mature and organized compared to CS-3% Fe_2O_3, CS and control group respectively. Control empty defects were not healed completely where a less mature bone was seen only along the periphery of the defect (Fig. 4e-h).

3.3.3. Histomorphometeric examination

Histomorphometric examination at one month revealed that mean ± SD values of immature bone area was 25.3 ± 4.9, 32.7 ± 8.0, 42.9 ± 9.3, and 61.6 ± 8.8 in control, CS, CS-3% Fe_2O_3, and CS-10% Fe_2O_3 respectively. A statistically significant increase ($P < 0.001$) in immature bone area in CS,

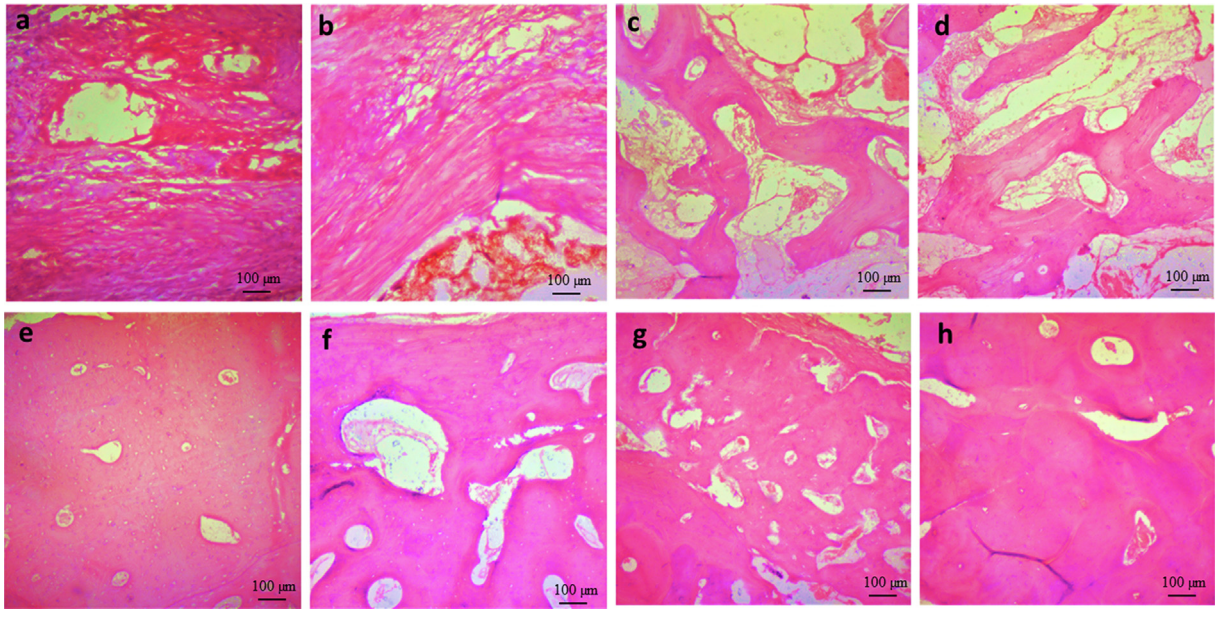

Fig. 3 Photomicrograph of induced mandibular defects at 1 months (a–d) and 3 months (e–h) following surgery. At 1 month, control defects were filled with loose connective tissue (a), calcium silicate group demonstrated filling of the defect site with dense connective tissue (b), 3 % calcium silicate-doped iron oxide group demonstrated areas of new bone formation (c), and 10% calcium silicate-doped iron oxide demonstrated interconnected bone trabeculae and osteoblasts were seen within bony trabeculae and on periphery (d). At 3 months, control defects were occupied by osteoid tissue (e), calcium silicate group defects occupied by bone tissue with osteoblastic proliferation (f), 3 % calcium silicate-doped iron oxide group defects showed filling of the defect with more organized bone tissue (g), and 10% calcium silicate-doped iron oxide group demonstrated mature bone formation with haversian canals (h) (H & E stain; Scale bar: 100 µm).

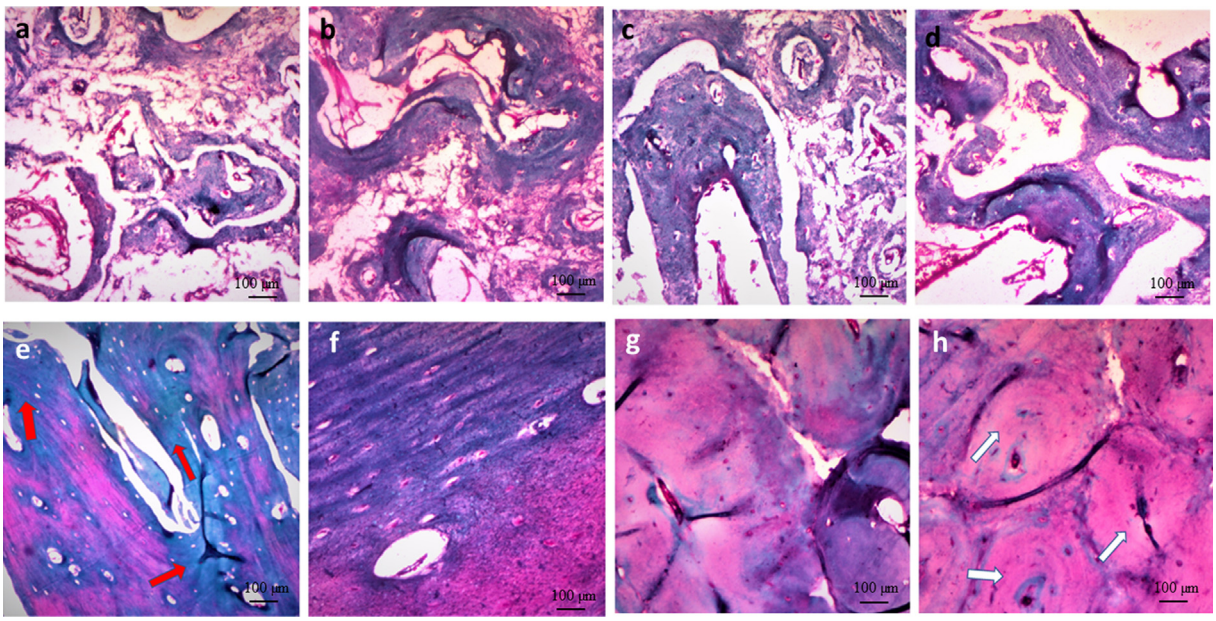

Fig. 4 Photomicrograph of induced mandibular defects at 1 months (a–d) and 3 months (e–h) following surgery. At 1 month, control defects showed loosely arranged connective tissue with small spicules of new bone (a), calcium silicate group demonstrated more organized connective tissue and more bone tissue (b), 3 % calcium silicate-doped iron oxide group had bone trabeculae with osteoblasts (c), and 10% calcium silicate-doped iron oxide group demonstrated interconnected bone trabeculae with osteoblasts (d). At 3 months, control defects showed immature bone (red arrows) with few osteoblasts in between (e), calcium silicate group demonstrated mature bone formation (f), 3 % calcium silicate-doped iron oxide group had more mature bone compared to calcium silicate group (g), and 10% calcium silicate-doped iron oxide group demonstrated complete mature bone formation (white arrows) (h) (Masson trichrome stain; Scale bar: 100 µm).

CS- 3% Fe_2O_3, and CS-10% Fe_2O_3 groups when compared to control defects. The percentages of increase (% change) of bone area were 22.7, 41.1 and 58.9% respectively. There was significant increase ($P < 0.001$) of immature bone at 1 month in CS-3% Fe_2O_3 and CS-10% Fe_2O_3 groups compared to CS group. Statistically significant increase in immature bone formation in CS-10% Fe_2O_3 group was recorded compared to CS- 3% Fe_2O_3 (Tables 1 and 2).

At three months, maturation of bone within defects was evident where mean ± SD values of mature bone was 2.66 ± 1.8, 9.9 ± 2.5, 22.9 ± 4.9, and 38.6 ± 8.1 in control, CS, CS-3% Fe_2O_3, and CS-10% Fe_2O_3 groups respectively.

A significant increase ($P < 0.001$) in area percent of mature bone was recorded in CS, CS- 3% Fe_2O_3, and CS-10% Fe_2O_3 groups compared to control group (73, 88 and 93.3% respectively). A significant increase ($P < 0.001$) in area of mature bone was recorded in 3% Fe_2O_3 and CS-10% Fe_2O_3 groups compared to CS group. Statistically significant increase ($P < 0.001$) in area of mature bone formation was detected in CS-10% Fe_2O_3 group compared to other groups.

The overall data revealed significant difference in the mean area percent of new bone formation in control group at one and three months that was the lowest mean followed CS, 3% Fe_2O_3 and CS-10% Fe_2O_3 groups. Although bone formation

Table 1 Mean, standard deviation (SD) and range of bone area percent at the induced mandibular defects of the control, calcium silicate, calcium silicate-3 % Fe_2O_3 and calcium silicate-10 % Fe_2O_3 groups obtained at one month (immature bone) and three months (mature bone) following surgery.

	Group	Mean area (%)	SD	Median	Range	F	P Value	% of Change
One month	Control [a]	25.3	4.9	24.5	19.3–34.6	39.47	< 0.001	0
	Ca Silicate pure [b]	32.7	8.0	30.9	21.7–48			22.7
	Ca silicate3% $Fe_2O_3^c$	42.9	9.3	44.5	29.6–58.2			41.1
	Ca silicate 10% $Fe_2O_3^d$	61.6	8.8	58.6	51.1–77.3			58.9
Three months	Control [a]	2.6	1.8	2.2	0.4–5.4	100.9	< 0.001	0
	Ca Silicate pure [b]	9.9	2.5	9.9	6.1–13.3			73
	Ca silicate3% Fe_2O_3 [c]	22.9	4.9	21.9	16.2–30.5			88
	Ca silicate 10% Fe_2O_3 [d]	38.6	8.1	41.1	26.6–49.3			93.3

Different superscript letters within the same time-point indicates statistically significant difference

Table 2 Inter-group comparison (Post hoc analysis) of the mean bone area percent of the different groups at one- and three-months following surgery.

	Group (X)	Group (Y)	Mean difference (X-Y)	P Value
One month	Ca silicate 10% Fe_2O_3	Control	36.3*	< 0.001
		Ca Silicate pure	28.9*	< 0.001
		Ca silicate3% Fe_2O_3	18.7*	< 0.001
	Ca Silicate Pure	Control	7.4*	0.043
	Ca silicate3% Fe_2O_3	Control	17.6*	< 0.001
		Ca Silicate pure	10.2*	0.007
Three months	Ca silicate 10% Fe_2O_3	Control	36.0*	< 0.001
		Ca Silicate pure	28.7*	< 0.001
		Ca silicate3% Fe_2O_3	15.7*	< 0.001
	Ca Silicate pure	Control	7.2*	0.002
	Ca silicate3% Fe_2O_3	Control	20.3*	< 0.001
		Ca Silicate pure	13*	< 0.001

* Statistically significant difference ($P < 0.05$).

was increased in all groups at one month compared to three months, bone quality and maturation was increased in all defects at 3 months.

4. Discussion

The present study demonstrated that addition of Fe_2O_3 nanoparticles to CS had a beneficial effect on bone regeneration compared to pure CS.

Physicochemical testing revealed that homogeneity of the chemical bonding was directly related to the band width. The strain in chemical bonds triggered small shift in band positions, which could change bond strength. The shift in band positions could be attributed to existence of Fe_2O_3 in the matrix, causing distortions of SiO_4 tetrahedral. The band at 770 cm^{-1} in the base is due to bending vibrations of Si—O bonds (Beherei et al., 2013). These vibrations appear almost damped in samples with 3 and 10% Fe_2O_3. The peaks corresponding to water molecules (H—OH) appeared at 3425 cm^{-1} (Mabrouk et al., 2019). A prominent absorption feature related to adsorption of water occurs at 1635 cm^{-1} could be accredited to the surface hydroxyl groups [H—O—H bending vibration of molecular H_2O] (Cornell and Schwertmann, 2006). The O—H bands can be used to categorize degree of crystallinity and degree of Fe-substitution, decreasing crystallinity causes broadening of the bands (Salama et al., 2015). Bands for CO_3^{-2} ν2 vibration were located at 680 and 1420 cm^{-1}, while the C═O appeared at 1600 cm^{-1} (Mahdy et al., 2021). For the highest content of 10% Fe_2O_3, the band at 638 cm^{-1} and shoulder at 695 cm^{-1} agreed well with maghemite (γ-Fe_2O_3) FTIR bands (Gotić et al., 2009; Lassoued et al., 2017).

Pre-clinical experiments are needed to verify biocompatibility, biofunctionality, biodegradability, osteointegration, osteoinduction and osteoconduction characteristics of bone substitutes. The dog is an ideal model for evaluating bone repair and testing bone substitutes (Taha et al., 2010, 2018; Mabrouk et al., 2021; Mostafa et al., 2021). In terms of bone size and weight, trabecular bone density, and bone turn over, the dog's macro- and micro-structure is very comparable to human bone, making it an appropriate model in pre-clinical setting (Abdel Hamid et al., 2020, 2021; Mostafa et al., 2021).

Critical-sized bone defects exceed the body's self-regeneration capabilities. The size of these defects varies depending on animal species, defective bone itself and on the integrity of the periosteum enclosing damaged bone. A 60-mm mandibular defect in presence of periosteum or a 15-mm in absence of periosteum has been identified to be critical-sized defect in dogs (Huh et al., 2005; Hosseinpour and Bastami, 2017).

CS has been used as biocompatible bone substitute with high mechanical resistance, and excellent bioactivity without evidence of carcinogenicity. A recent study investigated the *in vivo* cytotoxicity and biosafety of the CS-doped Fe_2O_3 nanoparticles to reconstruct mandibular defects in dogs. Results demonstrated no adverse histopathological changes within hepatic and renal tissue of dogs treated with CS-doped Fe_2O_3. It was concluded that CS-doped Fe_2O_3 nanoparticle is biologically safe and biocompatible. Additionally, CBCT scanning did not reveal any periapical or *peri*-disc radiolucency denoting absence of inflammation, infection, or necrosis within the surrounding bone in association with promoted bone regeneration (Mabrouk et al., 2021).

Silica ions promote osteoblastic proliferation during osteogenesis, indicating that silica is an essential element of bone cell function (Almeida et al., 2018). A previous study demonstrated that CS significantly promoted early bone formation compared to calcium phosphate (Wang et al., 2013). When compared to apatite-based composites, CS has an additional benefit in that it is more biodegradable and compatible. (Yuan et al., 2010; Jomova et al., 2012).

Iron and its alloys were used in orthopaedics where strong mechanical support was required (Finkemeier, 2002). Potential toxicity of excessive iron intake may be concerned, i*n vitro* and *in vivo* studies on iron-based implants demonstrated good biocompatibility and biosafety of pure iron (Liu and Zheng, 2011) while its slow biodegradability is a main disadvantage. Combination of iron with bioceramics with its high degradation rate can result in optimum results (Beger et al., 2018). Another possible approach is to enlarge the weight percentages or volume fractions of bioceramic particles added to the iron matrix

(Hermawan et al., 2010). Iron composites containing large amounts (20–40%) of CS particles were previously investigated, the composite containing 20% CS was superior to stimulate mesenchymal stem cell proliferation compared to pure iron suggesting that CS is effective in enhancing its biodegradation (Wang et al., 2016b). In the present study Fe_2O_3 nanoparticles (3% and 10%) promoted early healing compared to pure CS. Trace elements, like those found in bone, enhanced the osteogenic potential of CS. These results agree with Wang *et al.,* who reported positive influence of iron oxide nanoparticles on in vitro differentiation of mesenchymal stem cells into osteoblasts. The negative effect of iron on osteogenesis may be due to increased reactive oxygen species and ferritin activity, which was prevented by nanoparticle formulations (Wang et al., 2016a). The current study agreed with recent study by Mabrouk *et al*., who clarified the effect of iron oxide nanoparticles during radiological evaluation of Fe_2O_3/CS composites on bone healing (Mabrouk et al., 2021).

In contradiction, an inhibitory effect of iron on osteogenic lineage differentiation and no impact on chondrogenesis and adipogenesis was noted (Balogh et al., 2016). The promotion of osteoclast formation mediated by iron was previously reported, which additionally underscores the unfavourable features of iron in biomedical tissue engineering (Jia et al., 2012). Zhao *et al.,* analysed both effects of excessive and low body iron conditions on osteoblast activity (Zhao et al., 2012). Results illustrated that higher iron level inhibited osteoblastic activity depending on iron concentration, mild iron deficiency resulted in increased cellular activity, and severe deficiency of iron completely inhibited osteoblastic differentiation (Jeney, 2017). An enhanced osteoclast formation is one result of an increased iron concentration while osteogenic stimuli are blocked under the same conditions (Jeney, 2017). Further studies are recommended to clearly determine the potential benefits of iron in tissue engineering and the use of CS-doped iron oxide scaffolds in combination with autogenous bone graft and/or stem cells for bone formation.

5. Conclusion

Calcium silicate-doped iron oxide nanoparticles demonstrated promising synergistic effect by combining Fe_2O_3 nanoparticles to CS compared to CS alone in enhancing bone formation. CS-doped Fe_2O_3 are of good biocompatibility without adverse effect. Fe_2O_3 is a good osteoconductive composite providing an interconnected nano-porosity essential for bone ingrowth. It also provided feasible creeping substitution of new bone formation where nearly no remnants of graft material were left at 3 months following grafting. Increasing concentration of the doped Fe_2O_3 nanoparticles resulted in improved osteogenesis and bone maturation. The novel CS-Fe_2O_3 alloplasts could be effectively used for reconstruction of bone defects in oral and maxillofacial surgeries.

CRediT authorship contribution statement

Said K. Taha: Methodology, Writing – original draft, Project administration. **Mohamed A. Abdel Hamid:** Conceptualization, Methodology, Resources, Supervision. **Esmat M.A. Hamzawy:** Resources, Conceptualization, Validation. **Sayed H. Kenawy:** Conceptualization, Resources. **Gehan T. El-Bassyouni:** Conceptualization, Validation, Writing – review & editing, Supervision. **Elham A. Hassan:** Methodology, Investigation, Writing – review & editing. **Heba E. Tarek:** Visualization, Investigation, Data curation.

Declaration of Competing Interest

The authors declare that they have no known competing financial interests or personal relationships that could have appeared to influence the work reported in this paper.

Acknowledgement

The authors would like to thank Dr. Abdel Razik Farrag (Professor of General Pathology- National Research Centre), for his excellent assistance in the statistical analysis.

Funding

This research did not receive any specific grant from funding agencies in the public, commercial, or not-for-profit sectors.

Ethical statement

All study procedures were done in accordance with and approved by Animal Care and Use Ethical Committee of the National Research Center (approval #18121).

References

Abdel Hamid, M.A., Hassan, E.A., Zaied, A.A., Amaroli, A., Sorour, N.H., 2020. Dose-Dependent Clinical, Radiographic, and Histopathologic Changes of 17β-Estradiol Levels Within the Temporomandibular Joint: An Experimental Study in Ovariectomized Dogs. J. Oral Maxillofac. Surg. 78, 1304–1313. https://doi.org/10.1016/j.joms.2020.03.014.

Abdel Hamid, M.A., Zaied, A.A., Zayet, M.K., Abdelmageed, H., Hassan, E.A., Amaroli, A., 2021. Efficacy of Flat-Top Hand-Piece Using 980 nm Diode Laser Photobiomodulation on Socket Healing after Extraction: Split-Mouth Experimental Model in Dogs. Photochem. Photobiol. 97, 627–633. https://doi.org/10.1111/php.13356.

Alasmari, M.F., Dhaifullah, E., 2019. The roles of platelet rich plasma in bone grafts. Saudi Dent. J. 31, S11. https://doi.org/10.1016/j.sdentj.2019.02.007.

Almeida, M.S., Fernandes, G.V., Oliveira, A.M., Granjeiro, J.M., 2018. Calcium silicate as a graft material for bone fractures: a systematic review. Int. J. Med. Res. 46, 2537–2548. https://doi.org/10.1177/0300060518770940.

Altwaim, S., Al-Kindi, M., AlMuraikhi, N., BinHamdan, S., Al-Zahrani, A., 2021. Assessment of the effect of silica calcium phosphate nanocomposite on mesenchymal stromal cell differentiation and bone regeneration in critical size defect. Saudi. Dent. J. 33, 1119–1125. https://doi.org/10.1016/j.sdentj.2021.03.008.

Balogh, E., Tolnai, E., Nagy Jr, B., Nagy, B., Balla, G., Balla, J., Jeney, V., 2016. Iron overload inhibits osteogenic commitment and differentiation of mesenchymal stem cells via the induction of ferritin. BBA 1862, 1640–1649. https://doi.org/10.1016/j.bbadis.2016.06.003.

Beger, B., Blatt, S., Pabst, A.M., Hansen, T., Goetz, H., Al-Nawas, B., Ziebart, T., 2018. Biofunctionalization of synthetic bone substitutes

with angiogenic stem cells: Influence on regeneration of critical-size bone defects in an in vivo murine model. J. Craniomaxillofac. Surg. 46, 1601–1608. https://doi.org/10.1016/j.jcms.2018.06.002.

Beherei, H.H., Mohamed, K.R., El-Bassyouni, G.T., 2013. Mechanical and microstructure of reinforced hydroxyapatite/calcium silicate nano-composites materials. Mater. Des. 44, 461–468. https://doi.org/10.1016/j.matdes.2012.08.020.

Cornell, R.M., Schwertmann, U., 2006. The Iron Oxides: Structure, Properties, Reactions, Occurrence and Uses, second ed. Weinheim: Germany.

Finkemeier, C.G., 2002. Bone-grafting and bone-graft substitutes. J. Bone Joint Surg. Am. 84, 454–464. https://doi.org/10.2106/00004623-200203000-00020.

Gotić, M., Koščec, G., Musić, S., 2009. Study of the reduction and reoxidation of substoichiometric magnetite. J. Mol. Struct. 924–926, 347–354. https://doi.org/10.1016/j.molstruc.2008.10.048.

Hermawan, H., Purnama, A., Dube, D., Couet, J., Mantovani, D., 2010. Fe-Mn alloys for metallic biodegradable stents: degradation and cell viability studies. Acta Biomater. 6, 1852–1860. https://doi.org/10.1016/j.actbio.2009.11.025.

Hong, Y., Chen, X., Jing, X., Fan, H., Guo, B., Gu, Z., Zhang, X., 2010. Preparation, bioactivity, and drug release of hierarchical nanoporous bioactive glass ultrathin fibres. Adv. Mater. 22, 754–758. https://doi.org/10.1002/adma.200901656.

Hong, Y., Fan, H., Zhang, X., 2009. Synthesis and protein adsorption of hierarchical nanoporous ultrathin fibers. J. Physic. Chemi. B. 113, 5837–5842. https://doi.org/10.1021/jp9005444.

Hosseinpour, S., Bastami, F., 2017. Critical-Sized Bone Defects in Mandible of Canine Model. Tissue Eng. Part A 23, 470. https://doi.org/10.1089/ten.TEA.2016.0241.

Huh, J.-Y., Choi, B.-H., Kim, B.-Y., Lee, S.-H., Zhu, S.-J., Jung, J.-H., 2005. Critical size defect in the canine mandible. Oral Surg. Oral Med. Oral Pathol. Oral Radiol Endod. 100, 296–301. https://doi.org/10.1016/j.tripleo.2004.12.015.

Jeney, V., 2017. Clinical Impact and Cellular Mechanisms of Iron Overload-Associated Bone Loss. Front. Pharmacol. 8, 77. https://doi.org/10.3389/fphar.2017.00077.

Jia, P., Xu, Y.J., Zhang, Z.L., Li, K., Li, B., Zhang, W., Yang, H., 2012. Ferric ion could facilitate osteoclast differentiation and bone resorption through the production of reactive oxygen species. J. Orthop. Res. 30, 1843–1852. https://doi.org/10.1002/jor.22133.

Jomova, K., Baros, S., Valko, M., 2012. Redox active metal-induced oxidative stress in biological systems. Transit. Met. Chem. 37, 127–134. https://doi.org/10.1007/s11243-012-9583-6.

Lassoued, A., Dkhil, B., Gadri, A., Ammar, S., 2017. Control of the shape and size of iron oxide (α-Fe_2O_3) nanoparticles synthesized through the chemical precipitation method. Res. Phys. 7, 3007–3015. https://doi.org/10.1016/j.rinp.2017.07.066.

Liu, B., Zheng, Y.F., 2011. Effects of alloying elements (Mn Co, Al, W, Sn, B, C and S) on biodegradability and in vitro biocompatibility of pure iron. Acta Biomater. 7, 1407–1420. https://doi.org/10.1016/j.actbio.2010.11.001.

Mabrouk, M., ElShebiney, S.A., Kenawy, S.H., El-Bassyouni, G.T., Hamzawy, E.M., 2019. Novel, cost-effective, Cu-doped calcium silicate nanoparticles for bone fracture intervention: Inherent bioactivity and in vivo performance. J. Biomed. Mater. Res. B Appl. Biomater. 107, 388–399. https://doi.org/10.1002/jbm.b.34130.

Mabrouk, M., Taha, S.K., Abdel Hamid, M.A., Kenawy, S.H., Hassan, E.A., El-Bassyouni, G.T., 2021. Radiological evaluations of low cost wollastonite nano-ceramics graft doped with iron oxide in the treatment of induced defects in canine mandible. J. Biomed. Mater. Res. B Appl. Biomater. 109, 1029–1044. https://doi.org/10.1002/jbm.b.34767.

Mahdy, M.A., Kenawy, S.H., Hamzawy, E.M.A., El-Bassyouni, G.T., El Zawawi, I.K., 2021. Influence of SiC on Structural, Optical and Magnetic Properties of Wollastonite/Fe_2O_3 Nanocomposites. Ceramics International 9, 12047–12055. https://doi.org/10.1016/j.ceramint.2021.01.048.

Mostafa, A.A., Mahmoud, A.A., Abdel Hamid, M.A., Basha, M., El-Okaily, M.S., Abdelkhalek, A.F.A., El-Anwar, M.I., El Moshy, S., Gibaly, A., Hassan, E.A., 2021. An in vitro/in vivo release test of risedronate drug loaded nano-bioactive glass composite scaffolds. Int. J. Pharm. 607,. https://doi.org/10.1016/j.ijpharm.2021.120989 120989.

Salama, W., El Aref, M., Gaupp, R., 2015. Spectroscopic characterization of iron ores formed in different geological environments using FTIR, XPS, Mössbauer spectroscopy and thermoanalyses. Spectrochim. Acta A Mol. Biomol. Spectrosc. 136, 1816–1826. https://doi.org/10.1016/j.saa.2014.10.090.

Schmitz, J.P., Hollinger, J.O., 1986. The critical size defect as an experimental model for craniomandibulofacial nonunions. Clin. Orthop. Relat. Res. 205, 299–308. https://doi.org/10.1097/00003086-198604000-00036.

Taha, S.K., El Fattah, S.A., Said, E., Abdel-Hamid, M.A., Nemat, A. H., El Shenawy, H., 2018. Effect of Laser Bio-Stimulation on Mandibular Distraction Osteogenesis: An Experimental Study. J. Oral Maxillofac. Surg. 76, 2411–2421. https://doi.org/10.1016/j.joms.2018.04.030.

Taha, S.K., Yassin, S., Ayad, M., Farrag, A.H., Tawfik, W.A., Abbas, E.A., El-Bassyouni, G.T., 2010. Evaluation of osseous response to Bioglass/Dextran composite in induced mandibular defects: An experimental study. J.A.S.M.R. 5, 59–78.

Wang, C., Lin, K., Chang, J., Sun, J., 2013. Osteogenesis and angiogenesis induced by porous β-$CaSiO_3$/PDLGA composite scaffold via activation of AMPK/ERK1/2 and PI3K/Akt pathways. Biomaterials 34, 64–77. https://doi.org/10.1016/j.biomaterials.2012.09.021.

Wang, Q., Chen, B., Cao, M., Sun, J., Wu, H., Zhao, P., Xing, J., Yang, Y., Zhang, X., Ji, M., Gu, N., 2016a. Response of MAPK pathway to iron oxide nanoparticles in vitro treatment promotes osteogenic differentiation of hBMSCs. Biomaterials 86, 11–20. https://doi.org/10.1016/j.biomaterials.2016.02.004.

Wang, S., Xu, Y., Zhou, J., Li, H., Chang, J., Huan, Z., 2016b. In vitro degradation and surface bioactivity of iron-matrix composites containing silicate-based bioceramic. Bioact. Mater. 2, 10–18. https://doi.org/10.1016/j.bioactmat.2016.12.001.

Wei, J., Chen, F., Shin, J.W., Hong, H., Dai, C., Su, J., Liu, C., 2009. Preparation and characterization of bioactive mesoporous wollastonite-Polycaprolactone composite scaffold. Biomaterials 30, 1080–1088. https://doi.org/10.1016/j.biomaterials.2008.10.046.

Wu, C., Chang, J., Zhai, W., Ni, S., Wang, J., 2006. Porous akermanite scaffolds for bone tissue engineering: preparation, characterization, and in vitro studies. J. Biomed. Mater. Res. B Appl. Biomater. 78, 47–55. https://doi.org/10.1002/jbm.b.30456.

Yuan, H., Fernandes, H., Habibovic, P., de Boer, J., Barradas, A.M., de Ruiter, A., Walsh, W.R., van Blitterswijk, C.A., de Bruijn, J.D., 2010. Osteoinductive ceramics as a synthetic alternative to autologous bone grafting. PNAS 107, 13614–13619. https://doi.org/10.1073/pnas.1003600107.

Zhao, G.Y., Zhao, L.P., He, Y.F., Li, G.F., Gao, C., Li, K., Xu, Y.J., 2012. A comparison of the biological activities of human osteoblast hFOB1.19 between iron excess and iron deficiency. Biol. Trace Elem. Res. 150, 487–495. https://doi.org/10.1007/s12011-012-9511-9.